Pages: 30-40 / Vol. 19 / Issue 1 / Winter- Spring 2026

Journal of Aerospace Science and Technology

Journal Homepage: https://jast.ias.ir

Original Research Article

Numerical Simulation of Cold Flow in A Gas Combustion Chamber Sample with A New Design

Mohammad Mazidi Sharfabadi[1*], Ali Hosseini Moghadam Emami[2], and Seyed Mohammad Sadegh Mousavishad[3]

1*. Mechanical Engineering, Development and Optimization of Energy Technologies Division, Research Institute of Petroleum Industry (RIPI)

2. Iranian Research Organization for Science and Technology (IROST), Tehran, Iran

3. Islamic Azad University, Science and Research Unit, Tehran, Iran

ARTICLE INFO

Received: 31 December 2024
Revised: 11 May 2025
Accepted: 24 May 2025
Available online: 07 July 2025

KEYWORDS:

3.5 Series T56 motor
Combustion chamber
Gas turbine
Cold flow simulation
Cooling

DOI:
https://doi.org/10.22034/jast.2025.496857.1217

ABSTRACT

To enhance engine efficiency, extend the lifespan of components, and achieve more complete combustion, controlling the exhaust gases from the combustion chamber plays a crucial role in gas turbine design. This control can also be applied to cooling systems, which optimize the utilization of cooling air and improve the flow pattern within the combustion chamber. Notable progress has been made in the utilization of these systems. One of the latest models of combustion chambers is the T56 Series 3.5. While the general features of this chamber are identical to those of Series 3 and Series 2, the difference lies in the number and location of wall holes. Unfortunately, none of the manufacturer's technical specifications have been published. This paper aims to compare and assess the geometric and technical specifications of these chambers through numerical modeling, using the base model (T56 Series 3) as a reference. The localization of design knowledge for these chambers has been achieved. Simulation results indicate that flow rotation is almost eliminated in the secondary and dilution regions of the new chamber, and the thickness of the wall cooling layer remains nearly constant throughout the combustion chamber.

1 INTRODUCTION

In general, the design and optimization of a combustion chamber require many experiments, are time-consuming, and are expensive [1-2]. In alternative methods, the aim is to predict the overall pressure drop and flow distribution along the combustor instead of conducting costly tests. In one article [3], to predict the distribution of isothermal flow in the combustion chamber of a gas turbine, the pressure drop prediction of gas components is used. Graves and Grunman [4] presented diagrams to show the effect of different inlet parameters on the pressure drop and flow distribution in the combustion chamber. These diagrams were presented in other terms: reference Mach number of the chamber, the ratio of the

* Corresponding Author's Email: mazidim@ripi.ir

overall combustion temperature at the outlet to the inlet of the chamber, the percentage of air passing through the chamber, the ratio of the total area of the wall holes to the overall cross-sectional area of the chamber, and the ratio of the cross-sectional area of the chamber to the cross-sectional area of the outer shell. With the help of these diagrams, the effect of many geometries and performance conditions was mathematically investigated for compressible and incompressible flows. These diagrams are prepared for tubular combustion chambers with a constant cross-sectional area of the chamber and outer shell along the axis of the chamber. One of the most difficult issues in the design of a gas turbine is to obtain a suitable distribution of the exit temperature from the combustion chamber in a way that is acceptable for the turbine blades. The outlet temperature distribution is affected by various factors such as fuel nozzle characteristics, jet penetration, mixing, overall pressure drop along the chamber, dimensions, and shape. When the outlet temperature distribution is experimentally measured, the test should be performed at the maximum pressure that causes the maximum outlet temperature. The most important temperature for blades is the radial mean temperature distribution. This distribution is obtained by summing the temperature measured around each radius and then dividing it by the number of radii [5]. Another important parameter is the maximum space temperature, which controls the tension and corrosion of the guide vanes. The maximum of this temperature occurs between 50 and 70% of the radius [6]. A gas turbine combustor is a very complex combustion device. The challenge of designing these chambers is divided into two parts [7]: a) the development of models to describe the real geometric model, and b) an accurate description of the interaction between physical and chemical phenomena. Usually, to analyze a combustion chamber, first the boundary conditions are extracted from the empirical relationships of the flow in the holes, and then, with their help, the flow in the combustion chamber is modeled [1]. In addition, for the flow distribution inside the combustion chamber, the inlet flow angle in the cavities is predicted using the empirical relations shown by Lawson [1]. This method has weaknesses in at least two cases: it does not provide any information about the shape of the velocity distribution or the flow turbulence conditions, and the response obtained with this method is highly dependent on the accuracy of the boundary conditions [8]. When a computational fluid dynamics model and a one-dimensional model are combined, certain assumptions are made regarding the boundary conditions. An alternative method is the overall modeling of the combustion chamber. This perspective includes the modeling of the entire combustion chamber from the compressor outlet to the turbine inlet [9-12]. In this method, the flow through the holes and their boundary conditions are explicitly modeled, and there is no need for other assumptions. Also, when the flow on both sides of the chamber wall is modeled, the temperature of the chamber wall can be calculated [12]. In another study [13], a combination of the mentioned methods was used. Thus, by developing a one-dimensional code, the boundary conditions in the chamber cavities were first extracted and, after comparison with experimental data, were used as boundary conditions for modeling the internal flow. The pressure drop and temperature distribution at the exit from the combustion chamber were then extracted for different geometries of the combustion chamber. The new combustion chamber design, with new wall holes in terms of number, position, and size, is the main objective of this paper. For this purpose, the flow between the engine shell and the combustion chamber is numerically modeled, and the airflow rate from the holes and the flow distribution inside the combustion chamber will be calculated. To investigate the effect of changing the coordinates of the holes on the performance of the combustion chamber, numerical modeling has been done for both Series 3 and Series 3.5 combustion chambers, and their results have been obtained. All the studies conducted so far have been for the combustion chambers of Series 3 and earlier, and no information or research has been published yet for the combustion chamber of Series 3.5.

Recent advances in computational fluid dynamics (CFD) have significantly improved the design of gas turbine combustors. Zhang et al. (2020) employed large-eddy simulation to optimize hole distribution in annular combustors, demonstrating a 12% reduction in temperature non-uniformity [14]. Kumar and Lee (2021) applied adjoint-based optimization to a reverse-flow combustor, achieving improved dilution mixing [15]. More recently, Zhao et al. (2022) investigated variable hole geometry under operating transients, highlighting the benefits of adaptive cooling holes for thermal management [16]. Ahmed et al. (2023) used machine-learning-assisted surrogates to expedite design space exploration for hole patterns, reducing computational cost by 30% [17]. These studies underscore the importance of detailed hole geometry and cooling strategies in modern combustor design. Despite these advances, limited research exists on ground-up redesigns for legacy engines like the T56. This work fills that gap by comparing the established Series 3 chamber with a novel Series 3.5 design.

2 RESEARCH METHOD

In this study, a new cooling system for the chamber wall is proposed to improve the distribution of the cooling flow and dilution in the combustion chamber. This system, known as the Series 3.5, has been implemented by the manufacturer on the combustion chamber of the T56 engine. To evaluate the performance of the new model, the space between the external wall of the combustion chamber and the engine shell is numerically modeled, and the flow is compared with that of the base model.

3 MODELING ASSUMPTIONS

Steady-State and Compressible Flow

The simulation is performed under steady-state conditions, assuming compressible flow governed by the Navier-Stokes equations.

Turbulence Modeling

The Reynolds-Averaged Navier-Stokes (RANS) equations are used with the standard k−εk-\varepsilon k−ε and Realizable turbulence models to capture the turbulent characteristics of the flow.

Cold Flow Simulation

The study focuses on cold flow (non-reactive) conditions, analyzing cooling air distribution and velocity fields without combustion chemistry.

Flow Through Cooling Holes

Mass flow through each cooling hole is calculated using Bernoulli's principle and empirical discharge coefficients, considering pressure drop and hole geometry.

4 SERIES 3 COMBUSTION CHAMBER

For this purpose, the basic combustion chamber of Series 3 was first drawn based on the manufacturer's original drawings using SolidWorks software. The sketched model is shown in Figure 1.

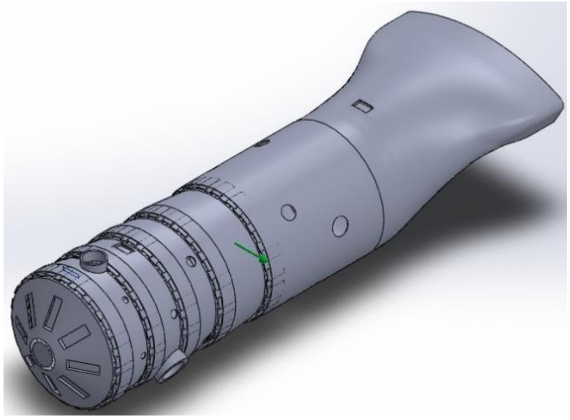

Figure1. The actual model of the basic combustion chamber of Series 3

A total of 12,000 different planes have been used to create the model with real geometry, as shown in Figure 1. During the grinding stage of the solution field, due to the small dimensions of these planes, the volume of the solution grid is greatly increased, which reduces the stability of the grid. As a result, the numerical solution becomes very complicated and time-consuming. The names of the holes in this chamber are given in Figure 2. The next step in preparing the 3D model of the problem is to draw the engine shell. Since the engine assembly consists of six combustion chambers arranged symmetrically around the engine axis, for the numerical analysis of the flow, it is sufficient to model one-sixth of the engine shell along with a combustion chamber. For this purpose, the engine shell is drawn based on the construction drawings and is shown in Figure 3.

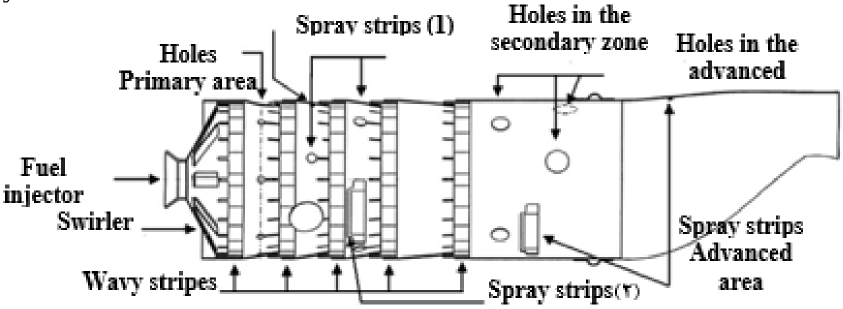

Figure 2. Schematic of the combustion chamber of Series 3

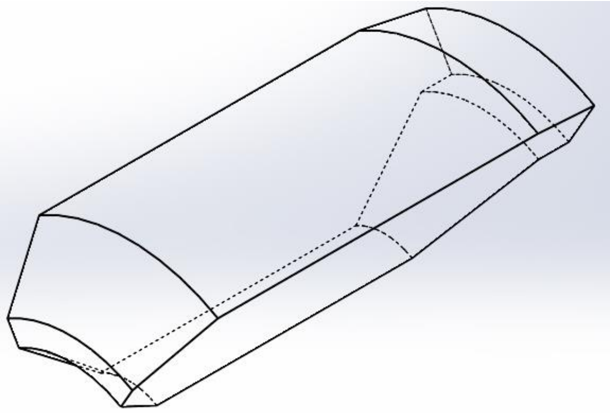

Figure 3. Isometric view of one-sixth cut of the engine cover

5 3.5 SERIES COMBUSTION CHAMBER

Today, a new design of the T56 engine's combustion chamber, known as the Series 3.5, is presented. Upon examining the combustion chamber of the Series 3.5, it becomes evident that the changes compared to the Series 3 are so extensive that it can be said that the foundation of the second design is completely different. These changes include the removal of the layered cooling devices, such as spraying and wavy strips, the uniformity of the external diameter of the combustion chamber, the reduction in the number of main holes, and the introduction of a large number of small holes with dual applications. In addition to providing the air required for combustion, flame stability, and controlling the output temperature of hot gases resulting from combustion, these holes are also used for cooling the combustion chamber wall. Despite these fundamental differences, there are important and practical similarities between both combustion chambers, such as the same external diameter, the same length, the same number of holes, the dimensions and shape of the exhaust submission chamber, and the rotors with equal entrance cross-sections. No information is available regarding the design and extraction of the geometrical parameters of the Series 3.5 combustion chamber. The only available image of this combustion chamber is shown in Figure 4.

Figure 4. A picture of the 3.5 series combustion chamber

According to Figure 5, the Series 3.5 combustion chamber can be divided into four different sections based on the longitudinal and circumferential pitch of the chamber holes. In the first section, named A, there are 5 rows of holes with a longitudinal pitch of 5 mm and a circumferential pitch of 3.75 degrees. In this area, the circumferential pitch around the chamber is constant. In section B, there are 24 rows of holes with a longitudinal pitch of 5 mm and a circumferential pitch of 2.72 degrees. The density of holes is higher in this area. Section C differs from sections A and B. The longitudinal pitch remains 5 mm, and the circumferential pitch is again the same as in the first section, 3.75 degrees. However, the circumferential pitch is not constant around the combustion chamber in section C. The hole density increases in two parts of this section, and the circumferential pitch reaches 2.72 degrees. These two regions are completely symmetrical. In the final section, the longitudinal pitch increases to 7 mm and the circumferential pitch to 7.5 degrees. In the peripheral regions, similar to section C, the circumferential pitch is also variable in this area. A general comparison between the two enclosures is provided in Table 1.

Table 1. General comparison between the combustion chamber series 3 and 3.5

District Primary	**Number of holes**		**Area of holes (mm^2)**	
	3	3.5	3	3.5
Secondary	95	659	1853	2638
Dilution	107	2601	2227	5085
The entire chamber	62	3032	2155	5412
District	264	6292	6235	13135

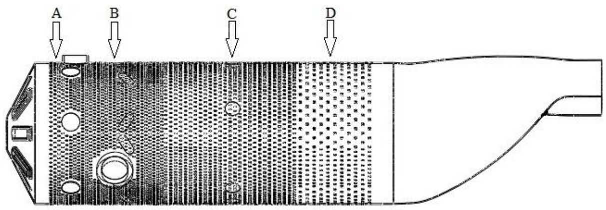

Figure 5. Schematic of the combustion chamber of the 3.5 series

6 MESHING

6.1 System specifications

Intel Core i7-5600 CPU, 8 cores, 24 GB RAM (as detailed in system configuration).

6.2 Simulation time for convergence

- **Series 3 model:** ~6–7 hours (steady-state)
- **Series 3.5 model:** ~7–9 hours
- **Geometry Modeling:** SolidWorks
- **Meshing:** ICEM
- **CFD Solver:** ANSYS Fluent 2015
- **Cell, T56 Series 3 model:**~1.2 to 1.5 million cells
- **Cell, T56 Series 3.5 model:**~2.0 to 2.5 million cells

7 SOLVING FIELD IN SERIES 3

Gambit software is used for meshing the solution field. The most critical part of any numerical modeling is the creation of a high-quality mesh. With meshing, the solution field is essentially divided into a volume of very small control volumes, consisting of cells and nodes. The quality of the mesh determines both the accuracy and the time required for the convergence of the solution. If the mesh is poorly constructed, the obtained results will either have low accuracy or will not converge at all. Generally, there are two types of meshing: structured and unstructured. The choice of each type depends on the geometric complexity of the model. The complex geometry of the solution field makes it impossible to use a structured mesh. In this study, the surface of the chamber is first meshed with unstructured three-dimensional cells of fixed size, and then a distribution function with an appropriate growth rate is used to reduce the size of the grid and shorten the solution time while maintaining accuracy. As a result, the mesh volume increases near the chamber, where high precision is required, and decreases with distance from it. Figure 6 shows the mesh of the solution field.

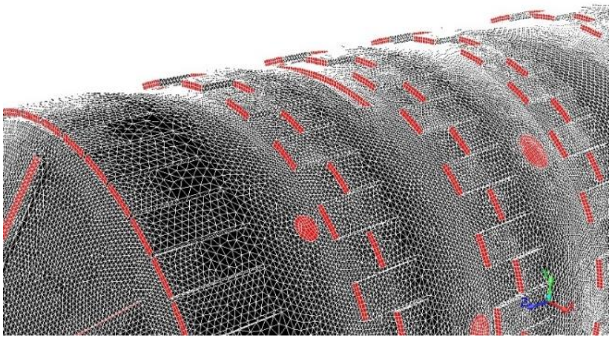

Figure 6. Liner surface meshing

8 SOLVING FIELD IN SERIES 3.5

On the surface of the combustion chamber, there are 6,292 holes, each with an area of only 1.55 mm^2. Therefore, to analyze the flow inside each hole, it is necessary to place at least two nodes inside each hole. According to the surface area ratio of each cavity to the surface of the combustion chamber, the maximum mesh size required on the surface, based on an appropriate growth rate of 1.2, will be equal to 0.15 square mm. On the other hand, since there is no symmetry in the model, the size of the mesh can be reduced. Consequently, with the same mesh dimensions, the minimum number of cells in the solution grid will be 18 million, which, in addition to making it impossible to reduce the number, also exceeds the computing memory limits of meshing software like GAMBIT and ICEM, making meshing unfeasible without sufficient computer memory. Furthermore, if the size of the cells increases outside the surface of the holes, the uniformity of the mesh will be lost. To address this issue, equivalent levels have been used, so that the input flow rate in each row is equal. In other words, the input flow rate from each considered equivalent level is equal to the total flow rate passing through all the holes in that row.

9 GOVERNING EQUATIONS

In the combustion chamber of a gas turbine, the mass and momentum transfer equations govern the flow. The most important aspect of the prevailing flow is the flow disturbances. Generally, turbulent flow is unsteady, with variable speed and properties .

The mass and momentum transfer equation for unsteady flow is [18]:

$$\frac{\partial \bar{\rho}\bar{u}_j}{\partial x_j} = 0 \quad (1)$$

$$\frac{\partial(\rho u_j)}{\partial t} + \frac{\partial}{\partial x_j}(\rho u_i u_j) = -\frac{\partial P}{\partial x_j} + \frac{\partial}{\partial x_j}\left[\mu\left(\frac{\partial u_j}{\partial x_i} + \frac{\partial u_i}{\partial x_j}\right)\right] + \rho g_i + F_i \quad (2)$$

Equation (2) is also known as the Navier-Stokes equation. The term F_i represents the volume forces of the flow. By using the time average of the flow properties, it is possible to obtain good information about the flow disturbances. To extract the flow properties, the flow velocity u (t) is divided into two components, the average velocity u¯ and the fluctuating velocity (u (t))´ [18]:

$$u = \bar{u} + u\acute{(}t) \quad (3)$$

If equation (3) is inserted into the Navier-Stokes equation, the Reynolds-averaged Navier-Stokes equation (RANS) is obtained [14]:

$$\frac{\partial(\rho \bar{u}_i)}{\partial t} + \frac{\partial}{\partial x_j}\left(\rho \bar{u}_i \bar{u}_j + \rho \overline{\acute{u}_i \acute{u}_j}\right) = -\frac{\partial P}{\partial x_j} + \frac{\partial}{\partial x_j}\left[\mu\left(\frac{\partial \bar{u}_j}{\partial x_i} + \frac{\partial \bar{u}_i}{\partial x_j}\right)\right] + \rho g_i + \bar{F}_i \quad (4)$$

By comparing relation (4) with the Navier-Stokes relation, a new component is observed, which is called Reynolds stress. Assuming that μ_t is constant, the new component is expressed as an equation (5) [18]:

$$-\left(\rho \overline{\acute{u}_i \acute{u}_j}\right) = \left[\mu_t\left(\frac{\partial \bar{u}_j}{\partial x_i} + \frac{\partial \bar{u}_i}{\partial x_j}\right)\right] - \frac{2}{3}\rho \delta_{ij} k \quad (5)$$

The turbidity viscosity coefficient μ_t is expressed by using the turbidity kinetic energy k and loss rate ε with equation (6) [18]:

$$\mu_t = C_\mu \rho \frac{k^2}{\varepsilon} \quad (6)$$

The RANS equations represent the perturbations for the mean value of the flow at each perturbation scale. The disturbance equations extracted from RANS equations are the standard k-ε model, RNG k-ε model, Realizable k-ε model, standard k-ω model, SST k-ω shear stress transfer model, and Reynolds RSM stress model. One of the basic models is the k-ε relation. This model has been used in a wide range and shows high matching results in different streams. However, it is not very accurate in some flows, such as undeveloped flows, rotating flows, and eddy flows. Although the standard k-ε model has problems in predicting vortices in the initial region of the jet, it has acceptable answers in other regions of the combustion chamber and in predicting the characteristics of the main flow of the combustion chamber. Due to the poor performance of this model in some simulations, some modifications have been made to predict the eddy currents better. RNG and Realizable models are two improved variants of the standard k-ε model. In this research, the RNG k-ε model is used. This model performs better than the standard mode in flows with low Reynolds and eddy currents. Relations (7) and (8) show the transfer equations for k and ε, respectively [18]:

$$\frac{\partial(\rho k)}{\partial t} + \frac{\partial}{\partial x_j}(\rho \bar{u}_j k) = \frac{\partial}{\partial x_j}\left[(\mu + \frac{\mu_t}{\sigma_k})\frac{\partial k}{\partial x_i}\right] + G_k - \rho\varepsilon \quad (7)$$

$$\frac{\partial(\rho \varepsilon)}{\partial t} + \frac{\partial}{\partial x_i}(\rho \bar{u}_i \varepsilon) = -\frac{\partial}{\partial x_i}\left[(\mu + \frac{\mu_t}{\sigma_\varepsilon})\frac{\partial \varepsilon}{\partial x_i}\right] + C_{1\varepsilon}\frac{\varepsilon}{k}G_k - C_{2\varepsilon}\rho\frac{\varepsilon^2}{k} \quad (8)$$

where G_k is the production rate of k:

$$G_k = -\rho \overline{\acute{u}_i \acute{u}_j}\frac{\partial u_j}{\partial x_i} \quad (9)$$

There are five different constants in relations 7 to 9. The value of these constants is extracted from the information collected from a wide range of flows, but the recommended values are [18]:
$C_\mu = 0.09$ $\sigma_k = 1$ $\sigma_\varepsilon = 1.3$ $C_{1\varepsilon} = 1.44$ $C_{2\varepsilon} = 1.92$

10 BOUNDARY CONDITIONS

In this article, according to the first objective, which is the cold analysis and calculation of the inlet flow rate from each cavity of the chamber wall, unlike previous studies, the space between the engine cover and the external surface of the combustion chamber has been modeled. Based on the flow conditions at the outlet of the compressor and the inlet to the combustion chamber, as presented in Table 2, the outlet pressure condition has been used for the holes on the surface of the chamber. This pressure is the same pressure that the flow entering the chamber will experience if combustion occurs in the chamber. For this purpose, considering that the pressure drop of the inlet flow in the combustion chamber is between 2 and 5%, the relative output pressure will be obtained at the surface of the chamber cavities.

Table 2. Flow conditions at the outlet of the compressor and inlet to the combustion chamber [19]

Parameter	Amount
Inlet temperature to the combustion chamber (K)	566.15
Inlet pressure to the combustion chamber (kPa)	923.897
Air flow mass flow rate (kg/s)	14.154

11 RESULTS AND DISCUSSION

11.1 Independence of results from networking the solution field in Series 3

In gridding the solution field, the smaller the grid size, the higher the accuracy of the solution. However, on the other hand, the duration of solving the problem and the specifications of the required hardware increase. Therefore, a balance must be established between the grid size, the accuracy of the solution, the time, and the required computing power. To investigate the effect of changing the grid size on the accuracy of the solution, three grids with low (705,283), medium (1,704,402), and high (2,354,528) densities have been created using an appropriate distribution function. As shown in Figure 7, the accuracy of the results for medium and dense grids is almost the same, but the results differ in the low-density grid. Since the convergence time in the dense grid is almost twice that of the medium grid, the medium grid with 3,584,762 cell walls and 1,704,402 volume cells has been used to analyze the results.

12 SOLVING FIELD IN SERIES 3.5

Similar to what was done for the Series 3 housing, three grids with dense (5,745,129), medium (3,371,097), and low-density (1,985,223) have been created to investigate the effect of changing the grid size on solution accuracy, using a suitable distribution function. As shown in Figure 8, the accuracy of the results for medium and dense grids is almost the same, but the results differ in the low-density grid. Since the convergence time in the dense grid is approximately 2.5 times that of the medium grid, the medium grid with 6,968,539 cell walls and 3,371,097 volume cells was used to analyze the results.

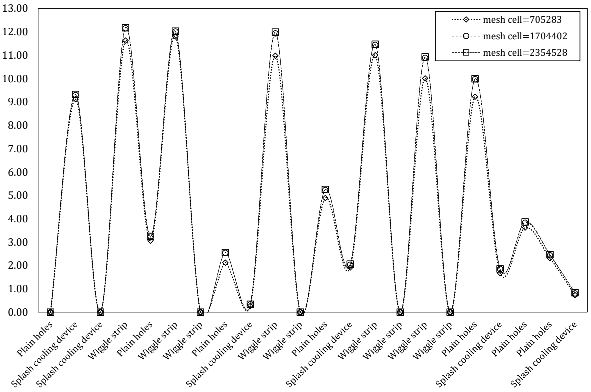

Figure 7. Results for the percentage of mass flow passing through the chamber holes in different solution networks

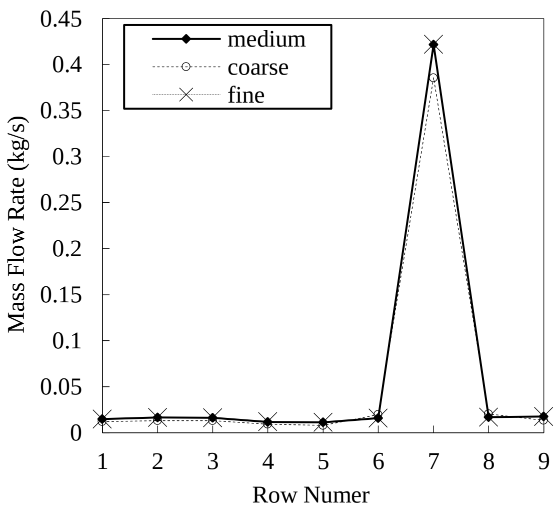

Figure 8. The results for the flow rate passing through the rows of the primary section of the 3.5 series combustion chamber in different solution networks.

13 VALIDATION OF NUMERICAL RESULTS

13.1 Solving field in series 3

Comparing the obtained results with experimental data shows the high accuracy of the results. The comparison between the numerical results of the Series 3 chamber and those of the developed one-dimensional code [13] is shown in Figure 9. Additionally, the comparison between the results obtained for the Series 3 chamber and the experimental results [20] is shown in Figure 10.

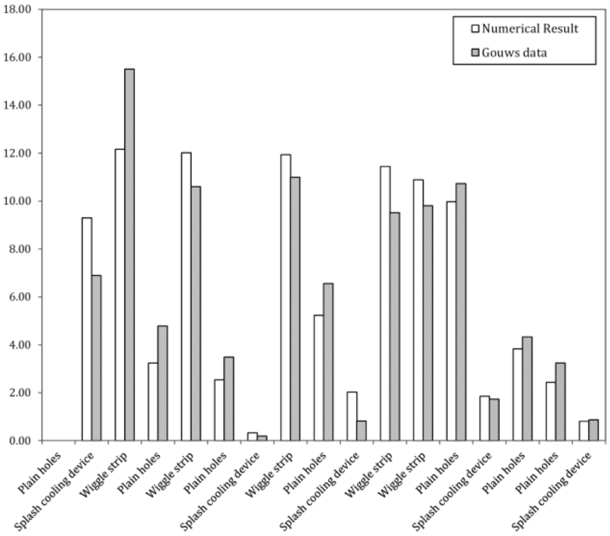

Figure 9. Comparison between the numerical results of the mass flow rate of series 3 chamber holes and one-dimensional Gauss code [13]

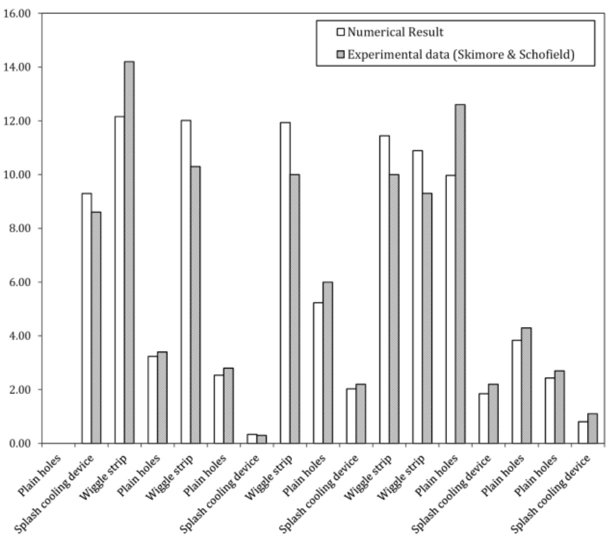

Figure 10. Comparison between the numerical results of the mass flow rate of the holes of the 3 series chamber and the experimental results [20]

13.2 Solving field in series 3.5

To validate the obtained numerical results, the results have been compared with the output of the one-dimensional code developed for the 3.5 series. This one-dimensional code was developed by Guzesi et al. [15] based on the one-dimensional Goos code. Figure 11 compares the mass flow distribution obtained from the present numerical work with the results of the one-dimensional code for the initial region of the 3.5 series combustor.

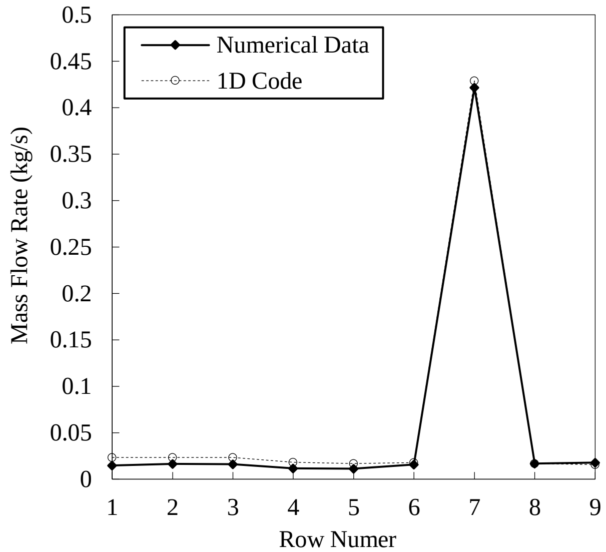

Figure 11. Comparison between the numerical results of the 3.5 series chamber and the one-dimensional code of Mazidi et al [19]

14 SERIES 3 CHAMBER RESULTS

The overall pressure contour of the solution field is shown in Figure 12, and the overall velocity vector is shown in Figure 13.

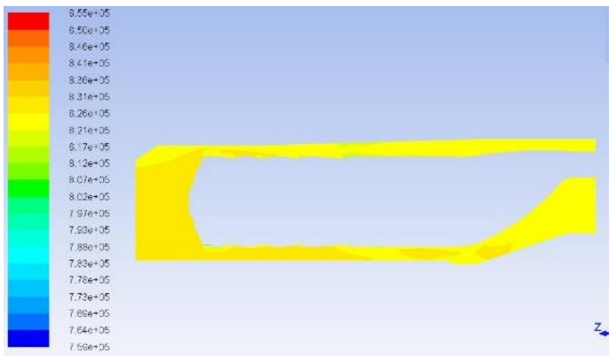

Figure 12. Total pressure contour in the solution field

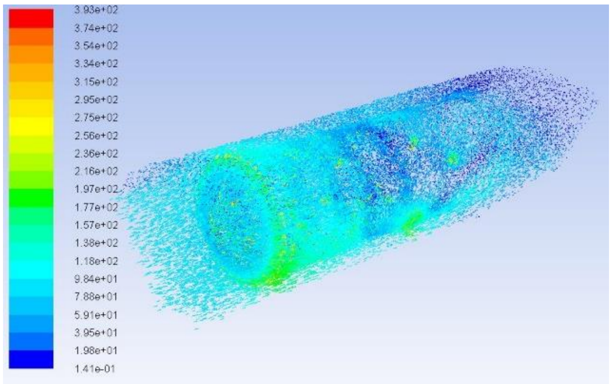

Figure 13. The overall velocity vector in the solution field

15 THE RESULTS OF THE 3.5 SERIES CHAMBER

Due to the identical dimensions of the Series 3 and 3.5 combustion chambers, the method used for the mass calculations of the Series 3 chamber can also be applied to the Series 3.5. Thus, when extracting and performing geometric modeling for numerical analysis, the initial pressure distribution is made equivalent to that of Series 3. The flow rate through each row of the Series 3.5 chamber cavity is shown in Figure 14.

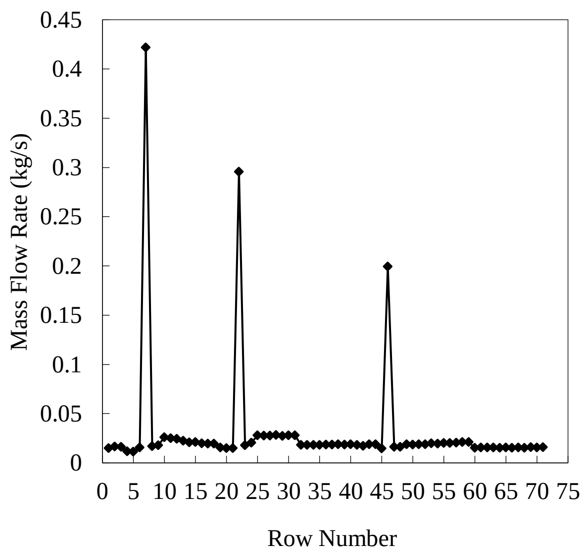

Figure 14. Diagram of passing mass flow rate in rows of combustion chambers of the 3.5 series

In this figure, it can be seen that the flow through each hole increases in the initial area as it moves along the combustion chamber. This increase continues up to row 7, which is the first row of primary holes, after which it starts to decrease until it enters the secondary area. In the secondary area, the flow rate from each hole decreases until row 22, which is the second row of main holes. After that, the flow rate increases again and enters the dilution area with an upward trend. In the dilution zone, the flow rate continues to increase, so that at the end of the combustion chamber and in the final rows, the flow rate passing through each hole reaches its maximum value.

16 COMPARISON OF INTERNAL CURRENTS OF SERIES 3 AND 3.5

After modeling the flow between the combustion chamber and the engine casing, the obtained pressure and flow rate at the combustion chamber inlets are used as boundary conditions for the cold solution of the internal flow field of the combustion chamber. After applying these boundary conditions and gridding the inner field of the solution, the same governing equations and discretization parameters used for the surrounding environment are applied. The results obtained are shown in Figures 15 and 16 for the Series 3 and Series 3.5 enclosures.

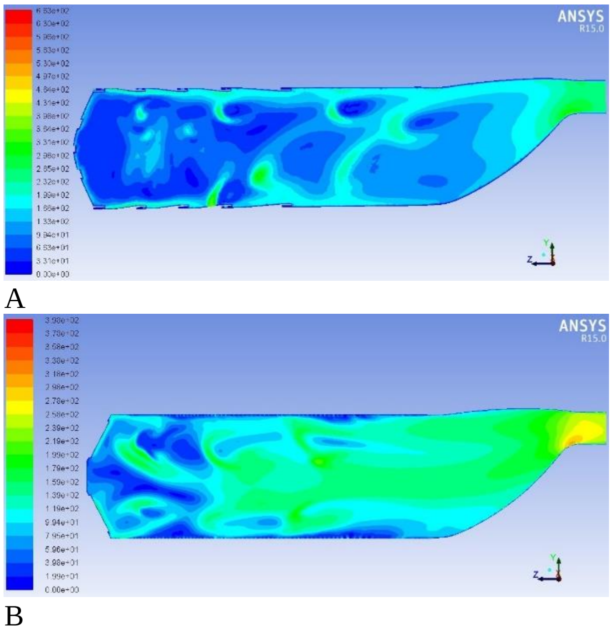

Figure 15. Overall velocity contour in the middle plane of the combustion chamber, (A) Series 3 and (B) Series 3.5

As shown in Figure 15, there are approximately three recirculation zones in the Series 3 chamber. These areas are almost eliminated in the Series 3.5 combustion chamber. Additionally, the internal cooling layer is evenly distributed throughout the

3.5 series chamber. The flow rate through different areas of both Series 3 and Series 3.5 chambers is shown in Table 3. These results represent the overall mass flow distribution in the primary, secondary, and dilution zones of both types of combustion chambers.

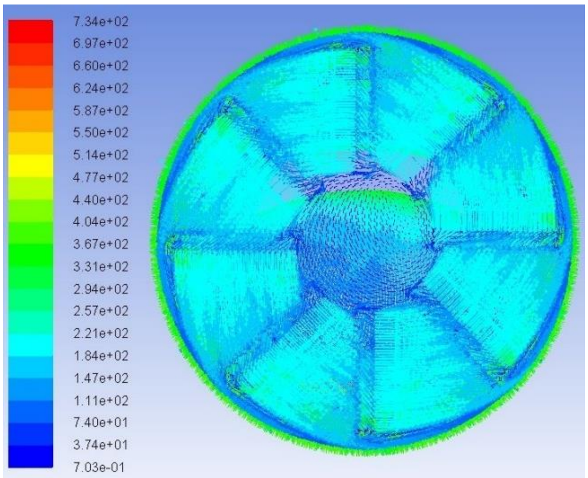

A

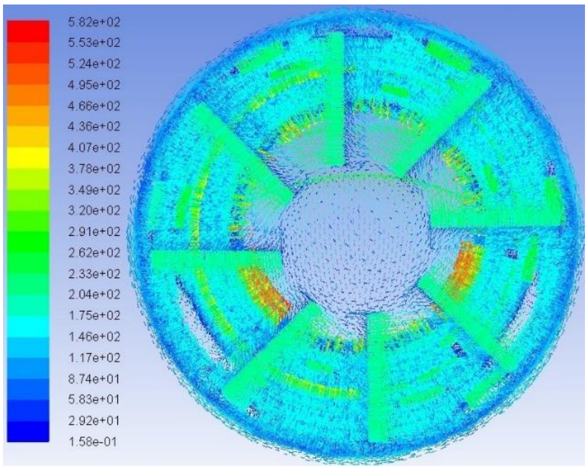

B

Figure 16. Overall velocity contour in the combustion chamber inlet plate, (A) Series 3 and (B) Series 3.5

Table 3. Comparison of the flow through the primary, secondary, and dilution areas of the combustion chamber of series 3 and 3.5

District primary	Mass flow rate (kg/s)	
	3	3.5
secondary	0.509	0.713
dilution	1.158	0.811
The entire chamber	0.707	0.855
District	2.374	3.37

17 SUMMARY AND CONCLUSION

In this article, the geometric model of the T56 Series 3 engine combustion chamber was first built, and a numerical analysis of the flow in the space between the combustion chamber and the engine casing was performed. As a result, the flow rate passing through all the holes and cooling tools was extracted and compared with experimental results, confirming the high accuracy of the obtained results. The T56 Series 3 engine combustion chamber was used as a base model to analyze the Series 3.5 combustion chamber and compare its performance with that of the Series 3. In this study, the Series 3.5 combustion chamber was numerically analyzed for the first time. The geometry of this chamber was extracted and geometrically modeled based solely on two available images. A numerical analysis of the flow in the space between the Series 3.5 combustion chamber and the engine casing was also performed. As a result, the flow through all the holes and cooling devices was calculated. A comparison was made between the flow through the primary, secondary, and dilution zones in both the Series 3 and Series 3.5 models. The results show an almost equal distribution of the input air between the three zones in the Series 3.5 combustion chamber. The analysis of the flow inside the combustion chamber was conducted for both Series 3 and Series 3.5. The results indicate that in the Series 3.5 combustion chamber, the flow in the secondary areas and dilution zones has nearly disappeared. Additionally, the thickness of the wall cooling layer in the Series 3.5 is almost constant throughout the combustion chamber.

CONFLICTS OF INTEREST

No potential conflict of interest was reported by the authors.

REFERENCES

[1] R. J. Lawson, “Computational Modeling of an Aircraft Engine Combustor to Achieve Target Exit Temperature Profiles”, ASME, No. 93, pp.164, 1993, https://doi.org/10.1115/93-GT-164

[2] N. C. Eccles, C. H. Priddin, *Accelerated Combustion Design using CFD*, ISABE pp No. 99-7094, 1999.

[3] H. A. Knight and R. B. Walker, “The Component Pressure Losses in Combustion Chambers”, Aeronautical Research Council R and M 2987, England, Report, 1953, https://reports.aerade.cranfield.ac.uk/handle/1826.2/3553.

[4] C. C. Graves, and J. S. Gronman, "Theoretical Analysis for Tubular Turbojet Combustors with Constant Annulus and Liner Cross-Sectional Areas", NACA Report 1373, 1957.

[5] A. H. Lefebvre, *Gas Turbine Combustion*, 2nd Edition, Taylor & Francis, 1998.

[6] D. S. Crocker and C. E. Smith "Numerical Investigation of Enhanced Dilution Zone Mixing in a Reverse Flow Gas Turbine Combustor", Journal of Engineering for Gas Turbine and Power, Vol. 177, pp 272-281, 1995, https://doi.org/10.1115/1.2814091.

[7] V. E. Tangirala, A. K. Tolpadi, AL. M. Danis, and H. Mongia, "Parametric Modeling Approach to Gas Turbine Combustor Design", *ASME*, No. 2000-GT-129, 2000, 10.1115/2000-GT-0129

[8] J. J. McGuirk, and A. Spencer, "Coupled and Uncoupled CFD Predictions of the Characteristics of Jets from Combustor Air Admission Ports", *Journal of Engineering for Gas Turbine and Power*, Vol. 123, pp 327-332, 2001, https://doi.org/10.1115/1.1362319.

[9] D. S. Crocker, D. Nickolaus, and C. E. Smith, "CFD Modeling of a Gas Turbine Combustor from Compressor Exit to Turbine Inlet", *Journal of Engineering for Gas Turbine and Power*, Vol. 121, pp. 89-95, 1999, https://doi.org/10.1115/1.2816318.

[10] J. J. McGuirk and J. M. L. M. Palma, "The Flow Inside a Model Gas Turbine Combustor: Calculations", *Journal of Engineering for Gas Turbines and Power*, Vol. 115, pp. 594-602, 1993, https://doi.org/10.1115/1.2906748.

[11] T. S. Snyder, J. F. Stewart, M. D. Stoner, and R. G. McKinney, "Application of an Advanced CFD-Based Analysis System to the PW6000 Combustor to Optimize Exit Temperature Distribution – Part II: Comparison of Predictions to Full Annular Rig Test Data", ASME pp 2001-GT-0064, 2001, https://doi.org/10.1115/2001-GT-0064.

[12] J. J., McGuirk and A.Spencer, "Coupled and Uncoupled CFD Prediction of the Characteristics of Jets from Combustor Air Admission Ports", ASME pp 2000-GT-0125, 2000,https://doi.org/10.1115/2000-GT-0125.

[13] J. J. Gouws, "Combining A One-Dimensional Empirical and Network Solver with Computational Fluid Dynamics to Investigate Possible Modifications to A Commercial Gas Turbine Combustor", Thesis for The Degree Master of Engineering, University of Pretoria, 2007.

[14] L. Zhan and et al. "LES Optimization of Annular Combustor Hole Distribution," *J. Propulsion Sci. Technol*., vol. 12, pp. 45–57, 2020.

[15] R. Kumar and H. Lee, "Adjoint-Based Optimization of Reverse-Flow Combustors," *Int. J. Heat Fluid Flow*, vol. 88, 108700, 2021.

[16] X. Zhao, et al. "Adaptive Cooling Holes for Transient Operations," Energy, vol. 237, 122123, 2022.

[17] S., Ahmed and et al. "Machine Learning Surrogates for Combustor Design," *Comput. Methods Appl. Mech. Eng*., vol. 379, 114742, 2023.

[18] M. H. Shojaeefard, M. Tahani, *An Introduction to Turbulent Flows and Its Modeling*, First Edition, Tehran: Iran University of Science and Technology Press, 2012. (In Persian).

[19] M. Mazidi Sharafabadi, S.M. Vaezi and E. Norouzi, "Performance and Emission Analysis of Combustion Chamber of a Turboprop Engine at Different Operation Regimes" *Sci. J. Fluid Mech. Aerodyn*. Vol. 4, No. 1, pp.65-75, 2015, (In Persian).

[20] F. W. Skidmore and W. H. Schofield, "The Variation in Airflow Cofficinet for Allison T56 Combustion Liners", *Defence Science and Technology Organisation*, Aeronautical Research Laboratories, Melbourne, Victoria, 1987.

HOW TO CITE THIS ATRICLE

M. Mazidi Sharfabadi, A. Hosseini Moghadam Emami and S. m. Sadegh Mousavishad, "Numerical Simulation of Cold Flow in A Gas Combustion Chamber Sample with A New Design," *Journal of Aerospace Science and Technology*, Vol. 19, Issue 1, 2026, pp. 30-40.

DOI: https://doi.org/10.22034/jast.2025.496857.1217

URL: https://jast.ias.ir/article_224359.html